Egyptian Journal of Radiology and Nuclear Medicine

RESEARCH

Open Access

Predictive quantitative multidetector computed tomography models for characterization of renal cell carcinoma subtypes and differentiation from renal oncocytoma: nomogram algorithmic approach analysis

Haytham Shebel[1*], Heba M. Abou El Atta[2], Tarek El-Diasty[1] and Doaa Elsayed Sharaf[1]

Abstract

Background Our objective is to develop an algorithmic approach using predictive models to discriminate between common solid renal masses, including renal cell carcinoma [RCC] subtypes and renal oncocytoma [RO], using multiphase computed tomography [CT].

Methods We retrospectively analyzed a group of solid renal masses between January 2011 and January 2023 regarding the CT attenuation values using a multiphase multidetector CT and clinical parameters. Inclusion criteria included patients who had four phases of CT with a partial or radical nephrectomy. Exclusion criteria were patients with biphasic or one-phase CT, poor imaging quality, patients under surveillance, radiofrequency ablation, or indeterminate pathology findings as oncocytic tumor variants. We divided our cohort into training and internal validation sets.

Results Our results revealed that a total of 467 cases, 351 patients assigned for the training cohort and 116 cases assigned for validation cohort. There is a significant difference between hypervascular clear RCC [CRCC and RO] and hypovascular chromophobe and papillary [ChRCC and PRCC] masses in both training and validation sets, AUC = 0.95, 0.98, respectively. The predictive model for differentiation between CRCC and RO showed AUC = 0.83, 0.85 in both training and validation sets, respectively. At the same time, the discrimination of ChRCC from PRCC showed AUC = 0.94 in the training set and 0.93 in the validation cohort.

Conclusions Using the largest sample to our knowledge, we developed a three-phase analytical approach to initiate a practical method to discriminate between different solid renal masses that can be used in daily clinical practice.

*Correspondence:
Haytham Shebel
haythamshebel@gmail.com
Full list of author information is available at the end of the article

Key points

1. This study aims to differentiate between malignant and benign renal masses.
2. Computed tomography with new approach can solve this issue.
3. *Multiphasic CT can predict malignant probability with high accuracy.*

Keywords Carcinoma, Renal cell, Nomograms, Chromophobe, Papillary, Oncocytoma, Renal

Background

Universally, renal cell carcinoma [RCC] represents 5% and 3% of all urological malignancies in men and women [1]. The incidence of RCC diagnosis has increased since 1990 without clear, definite reasons. One of the reasons for such a rise is due to an increase in incidental detection by using imaging modalities, especially computed tomography [CT] [2]. The three commonest subtypes of RCC include clear cell [CRCC] [75–80%], papillary type [PRCC] [14–17%], and chromophobe [ChRCC] [4–8%] [3]. There are established imaging features for RCC diagnosis, and some features may identify its subtypes. However, the current imaging techniques still have controversy and weak accuracy in differentiating RCC from benign masses such as renal oncocytoma [RO], which arises from the collecting duct and accounts for 3–5% of all solid renal masses [4–7]. The similarity of origin and pattern of enhancement between RCCs and ROs may contribute to the difficulty of this differentiation in the preoperative stage. Therefore, the definite diagnosis is based on histopathologic analysis of the surgically removed mass rather than imaging [4].

Accordingly, preoperative imaging diagnosis is of special importance to avoid unnecessary kidney resection or benign tumor. In the last few years, there has been a growing concept of less aggressive management, including active surveillance for the small renal masses even if they were diagnosed as malignant because they could be low-grade RCCs with low potential morbidity [8, 9]. On the other hand, new treatment options such as target and immune therapy are developing for advanced cases [10]. For all those reasons, the characterization, stratification of RCC subtypes, and their differentiation from benign RO have necessary implications in clinical practice. Therefore, there were many attempts to develop and enhance the imaging techniques to predict this differentiation in the preoperative stage. Some studies utilized quantitative, and others used qualitative CT features for differentiation [11–13].

In the last few years, the introduction of machine learning and textural analysis to differentiate between RCC subtypes has had promising results [14–17]. However, due to the different techniques and multiple productions of different radiomics software, in addition to the need for highly expert individuals with different levels experience that produce wide variability in the utilized features, no standard methods could be achieved [18, 19].

Furthermore, other studies tried to develop multivariable predictive models to enhance the differentiation between RCC subtypes, and other studies included RO using different separate variables [20, 21]. However, these studies examined a small sample size with incomparable numbers of tumors at the different arms. Unlike previous studies, we included the largest sample size in different RCC subtypes and RO to our knowledge.

As a result, we intend to develop a stepwise analytical approach based on multiple predictive models, including the best classifiers, by creating training and validation cohorts using multiphase CT parameters for the most common types of RCC and attempting to distinguish them from RO.

Methods

Patients

The institutional review board approved this retrospective study, and informed consent was waived. We searched our medical records from January 2011 to January 2023 for patients with proven pathology for various RCC subtypes and RO.

Patients with four phases of CT and a partial or radical nephrectomy met the inclusion criteria. Patients with biphasic or one-phase CT, poor imaging quality, patients under radiofrequency ablation, surveillance, or uncertain pathology results as an oncocytic tumor variant were excluded.

Finally, we identified 467 cases with the final diagnosis of RO and different subtypes of RCC.

CT Examinations

The examinations were carried out using a multidetector CT scanner with 64 parallel detector rows (Brilliance CT; Philips Medical Systems Nederland, Veenpluis 4–6, the Netherlands) and post-processing was carried out on a (Brilliance; Philips) workstation V3.01.5000. Patients were advised to refrain from eating or drinking for two

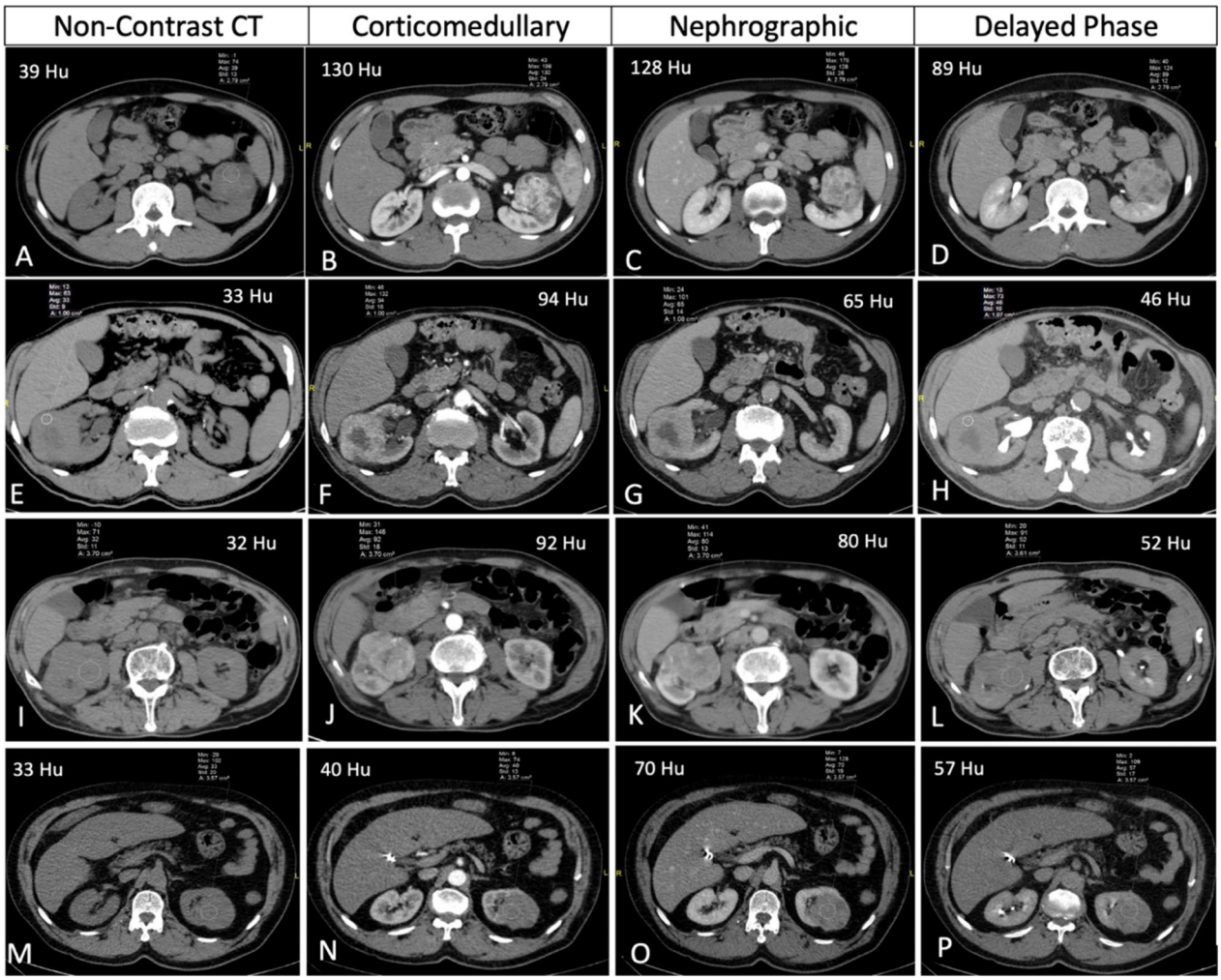

Fig. 1 Axial scans of the abdomen of a case of renal cell carcinoma clear cell type (**A**–**D**), oncocytoma (**E**–**H**), chromophobe renal cell carcinoma (**I**–**L**), and papillary renal cell carcinoma (M-P), with average attenuation values at non-contrast, arterial, venous, and delayed phases

hours prior to the scan, and no oral contrast was administered. Intravenous contrast [100–120 ml nonionic contrast, concentration 300 mg/ml] was injected at a rate of 4 ml/sec using a mechanical injector. During the non-contrast and venous phases, patients were scanned from the diaphragm to the symphysis pubis, and during the arterial and delayed phases, they were scanned via the kidney region.

The scanning parameters were as follows: tube voltage, 120 kVp (all phases); tube current, average 220 mA; slice thickness, 2.5 mm; reconstructed thickness, 5 mm; pitch, 0.984; rotation period, 0.75 s. The four CT phases were non-contrast, arterial, venous, and delayed. The arterial phase was delayed by 25–40 s, the parenchymal phase by 85 s, and the delayed phase by 300–420 s. All patients had their scans reconstructed in the axial, sagittal, and coronal planes.

Image analysis

Attenuation values in Hounsfield units [HUs] and regions of interest [ROI] were measured entirely within the solid part of the mass, avoiding the periphery or any areas with calcification, cystic degeneration, or visible vasculature. In each CT phase, three ROIs with a range of [13–20 mm] were applied to each tumor, and one average value was obtained (Fig. 1). Variations in lesion enhancement, or absolute enhancement [AE], were computed by subtracting the non-contrast phase's attenuation value from the post-contrast phase's attenuation value. Tumor size was calculated using the largest diameter in either the sagittal or coronal reformatted images. These measurements were taken by consensus by two highly experienced radiologists [El-Diasty T and Shebel H] who had 35 and 25 years of experience reporting genitourinary CT images, respectively]. The final pathology reports were

not disclosed for them. They examined the scans at a certain workstation (Advantage Window 4.1; Philips).

Statistical analysis

Our outcome was tumor discrimination and validation. Our cohort was randomly divided into a training cohort and an internal validation cohort with a 75:25 ratio using random numbers. Age, size, gender, attenuation values, and AE of the tumors in four different CT phases were used as predictors. The mean and standard deviation were used as estimation points for continuous variables. For categorical variables, the frequency. The Shapiro–Wilk test was used to determine the data's normality. A Student t test was used to determine whether there was a significant difference between tumor types in terms of age, size, gender, and attenuation values. We developed three phases of analysis. The goal of phase I is tumor categorization into hypervascular and hypovascular groups by using longitudinal analysis for each study phase for all tumors. The odds ratio of association between tumor vascularity and the aforementioned predictors was then predicted using logistic analysis. Our goal in phases II and III was to distinguish between tumor types that belonged to each group, hypervascular or hypovascular. To identify the most significant combination for tumor characterization, stepwise variable selection was used. The area under the curve [AUC] was plotted and estimated after determining the most significant independent predictors for each phase. The area under the curve and the odds ratio of the final version, with 95% confidence intervals, are reported. For all statistical tests, a *P* value of less than 0.05 was considered statistically significant. After determining the best classifiers for each phase of the analysis, a nomogram was created to provide a visual predictive tool. Statistical analyses were carried out using the STATA/IC version 16.1 software package.

Table 1 Demographic distribution and CT parameters of the training cohort

Subtype	(Number)	(mean)	(median)	(SD)	(max)	(min)
Clear						
Age	147	53.7551	54	10.55098	83	18
Sex	147	0.6326531	1	0.4837303	1	0
Size	147	7.446939	7	3.218979	18	2
artHU	147	122.1633	120	35.24572	239	62
venousHU	147	101.2789	100	24.7668	190	55
delayedHU	147	64.73469	64	14.59186	120	41
Oncocytoma						
Age	61	59.42623	60	10.3802	76	30
Sex	61	0.442623	0	0.500819	1	0
Size	61	6.740984	5.8	3.145864	16	3
artHU	61	93.47541	96	22.28498	163	53
venousHU	61	98.52459	95	21.84003	154	60
delayedHU	61	63.2623	65	13.65272	115	40
Chromophore						
Age	92	51.3913	51	11.75478	81	22
Sex	92	0.5543478	1	0.4997611	1	0
Size	92	8.726087	8.55	3.65537	19	2.5
artHU	92	73.17391	70	19.22716	125	35
venousHU	92	75.19565	76.5	14.86883	110	47
delayedHU	92	53.84783	53	11.44114	84	27
Papillary						
Age	51	53.45098	52	10.81538	79	31
Sex	51	0.7254902	1	0.4507075	1	0
Size	51	6.503922	6	2.762532	14	3
artHU	51	45.60784	43	14.23106	83	21
venousHU	51	61.84314	59	15.18074	114	40
delayedHU	51	52.33333	50	12.80104	97	30

Table 2 Demographic distribution and CT parameters of the validation cohort

Subtype	number	mean	median	SD	max	min
Chromophore						
Age	32	51.46875	52.5	11.13838	70	23
Sex	32	0.5	0.5	0.5080005	1	0
Size	32	9.034375	8.3	3.660302	16.5	4
artHU	32	77.25	71	21.26788	125	45
venousHU	32	79.59375	80	15.21642	119	37
delayedHU	32	56.78125	54.5	12.24148	97	37
Clear						
Age	48	53.16667	52.5	10.90058	76	19
Sex	48	0.7291667	1	0.4490929	1	0
Size	48	8.7125	9	4.219793	21	2.5
artHU	48	118.6042	124	27.21681	180	69
venousHU	48	100.9792	101	19.75649	155	55
delayedHU	48	63.83333	62	12.06954	90	35
Oncocytoma						
Age	20	56.25	59	14.60308	76	30
Sex	20	0.6	1	0.5026247	1	0
Size	20	6.155	5.85	1.499289	9.5	4
artHU	20	95.5	99.5	25.01052	145	39
venousHU	20	93.95	90	16.48436	141	78
delayedHU	20	62.95	66.5	12.98775	83	45
Papillary						
Age	16	55.375	55.5	13.36101	76	32
Sex	16	0.875	1	0.341565	1	0
Size	16	6.58125	5.25	3.690026	17	2
artHU	16	47.875	47	9.708244	66	30
venousHU	16	58.3125	59	7.471892	70	42
delayedHU	16	49.0625	45.5	10.66751	81	40

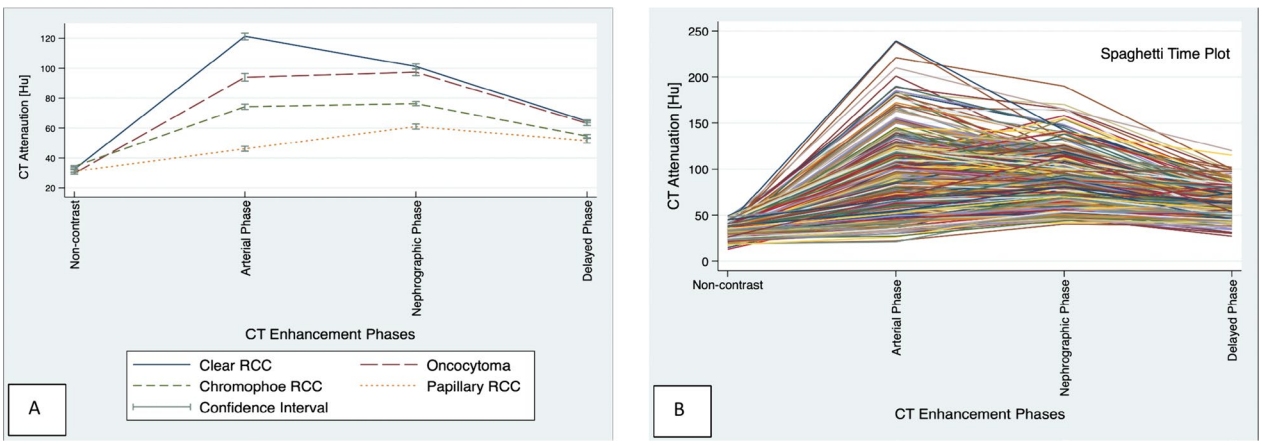

Fig. 2 A,B: **A** longitudinal analysis curve shows the significant difference in the attenuation mean of the different pattern of the renal masses, in the four phases of the CT study. **B** Spaghetti Time Plot curve shows the individualized renal masses attenuation enhancement pattern

Results

Our results revealed a total of 467 cases were included in the final analysis, with 351 patients assigned to the training cohort [mean age, 54 + 11 years; 147 CRCC, 61 RO, 92 ChRCC, and 51 PRCC] and 116 patients assigned to the internal validation cohort [mean age, 53 + 12 years; 48 CRCC, 20 RO, 32 ChRCC, and 16 PRCC]. The demographic data, including the mass distribution, age, frequency between genders, and the mean attenuation value regarding CT parameters in both training and validation cohorts, are illustrated in Tables 1 and 2.

We established three phases of analysis to build a practical approach that can be used in daily clinical practice.

Statistical analysis revealed that the attenuation means and the absolute means showed identical correlation and significance in all phases of analysis; therefore, the absolute mean values were backward from analysis. To assess the generalization ability of the model, there were no significant differences between both cohorts regarding age, size, sex, or mean attenuation values.

Phase I

Categorization based on tumor vascularity

We used longitudinal analysis to examine the enhancement pattern in all tumor types, which revealed that CRCC and RO have higher significant enhancement values than ChRCC and PRCC in arterial, venous, and delayed phases, with p value [< 0.001] for all phases. Additionally, there is a significant difference in the non-contrast phase, p value [0.004], Fig. 2 Therefore, we categorize the included masses into hypervascular and hypovascular groups.

Discrimination model and validation for hypervascular and hypovascular masses

Clinical predictor variables Age as a clinical predictor showed a significant difference between both groups, p value [0.009]. The mean age of the hypervascular masses was higher [55 years] compared with the hypovascular masses [52 years]. In contrast, sex and the size of the tumors did not show a significant difference between both groups, p value [0.781], and p value [0.075], respectively. Univariable analysis for the age showed a positive association with the hypervascular masses, with an odds ratio [1.02], and a p value [0.007].

Development and validation of the final model of phase I Multivariable logistic model for attenuation values in the four phases of the CT study showed that arterial and venous attenuation had a significant positive association with hypervascular masses. In contrast, non-contrast and delayed attenuations exhibit a significant negative association with tumor hypervascularity; the coefficient and P values are shown in Table 3. This model had a high AUC [0.94] for discrimination between renal masses based on vascularity pattern. Including age as the only clinically significant predictor in the final model gives a higher AUC [0.95] for discrimination between both groups. The arterial and venous attenuations had higher odds of prediction (1.10 and 1.05, respectively). Applying this model to the validation cohort yields a higher AUC [0.98] for such discrimination Fig. 3.

Phase II

Discrimination model and validation for hypervascular masses [CRCC Vs. RO]

Renal oncocytoma and CRCC were involved in this group. Univariable logistic analysis of the above predictors revealed age, sex, size, non-contrast, and arterial and delayed attenuations were significantly associated with the tumor types. In contrast, venous attenuations showed no significant association Table 4. While age and delayed attenuations had a negative association with CRCC, the remaining predictors showed a positive relationship with CRCC. Further multivariable analysis to build the best model included the above significant predictors revealed; the size had no longer significant correlation; thus, it was excluded from this model. For clinical predictors including age and sex, the AUC was [0.67]. However, the combination of these predictors [age and sex] with the significant attenuation predictors, [non-contrast, arterial, and delayed HU] produced the best final model

Table 3 Significant predictors used to categorize the masses into hypervascular and hypovascular groups

Vascularity	Coefficient	Std. Err	Z	P-value	[95% Conf. Interval]	
artHU	0.0941883	0.0134332	7.01	0.000	0.0678598	0.1205168
nocontrastHU	−0.1852756	0.0390239	−4.75	0.000	−0.261761	−0.1087902
age	0.0470496	0.0168577	2.79	0.005	0.0140092	0.08009
venousHU	0.0480014	0.0147197	3.26	0.001	0.0191512	0.0768515
delayedHU	−0.0540809	0.0213912	−2.53	0.011	0.0191512	−0.0121549
_cons	−3.600522	1.717373	−2.10	0.036	−6.966512	−0.2345319

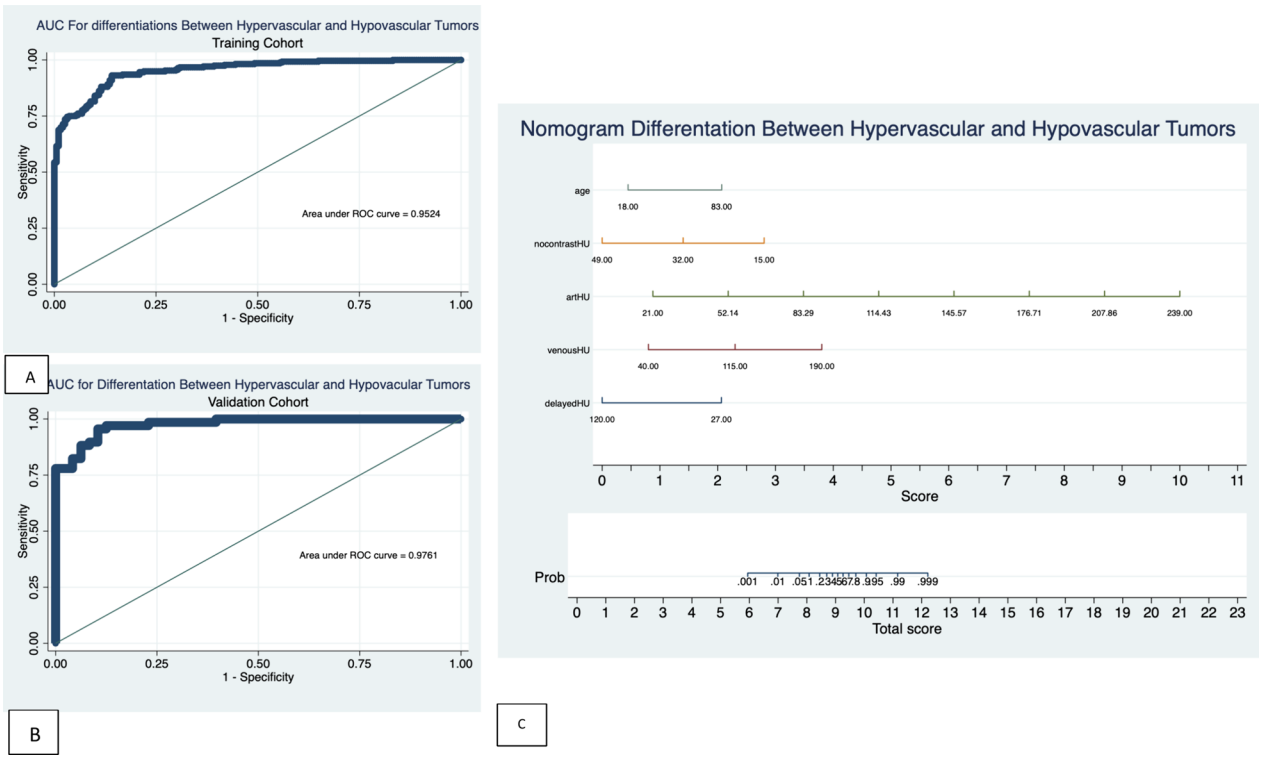

Fig. 3 A,B, and C: **A** AUC of the training cohort with accuracy = 0.95 for discrimination between hypervascular and hypovascular groups. **B** AUC of the validation cohort with accuracy = 0.98 for discrimination between hypervascular and hypovascular groups. **C** Nomogram using the significant predictors that can classify between both groups

Table 4 Significant predictors used to discriminate between hypervascular masses [CRCC Vs. RO]

hypotumor	Coefficient	Std.Err	Z	P-value	[95% Conf. Interval]	
artHU	0.0534177	0.0102644	5.20	0.000	0.0332999	0.0735355
delayedHU	−0.0712916	0.0187747	−3.80	0.000	−0.10808939	−0.0344938
Age	−0.0602021	0.0197716	−3.04	0.002	−0.0989537	−0.0214505
Sex	1.009846	0.3809394	2.65	0.008	0.2632182	1.756473
nocontrastHU	0.0827004	0.0365006	2.27	0.023	0.0111605	0.1542402
_cons	0.0472721	1.739649	−0.03	0.978	−3.362376	3.456921

describing the data, with an AUC value of [0.83] in the training set and [0.85] in the validation cohort Fig. 4.

Phase III

Discrimination model and validation for hypovascular masses [ChRCC Vs. PRCC]

Regarding hypovascular masses, while age, sex, noncontrast, and venous attenuation showed no significant differences between tumor subtypes, size, arterial, and delayed attenuation showed a significant association between both subtypes Table 5. Both size and arterial attenuation revealed positive associations with ChRCC; delayed attenuation showed a negative association. The multivariable analysis revealed that the above three predictors showed the best model for tumor type discrimination for this group, with a high AUC value of 0.94 and 0.93 in the training and validation cohorts, respectively Fig. 5.

For each phase of the analysis, a nomogram chart was created using the best classifiers predictors as a primarily graphical tool Figs. 3, 4, and 5. Finally, we developed a diagram describing the core analysis of the above three phases, illustrating the significant predictors in each

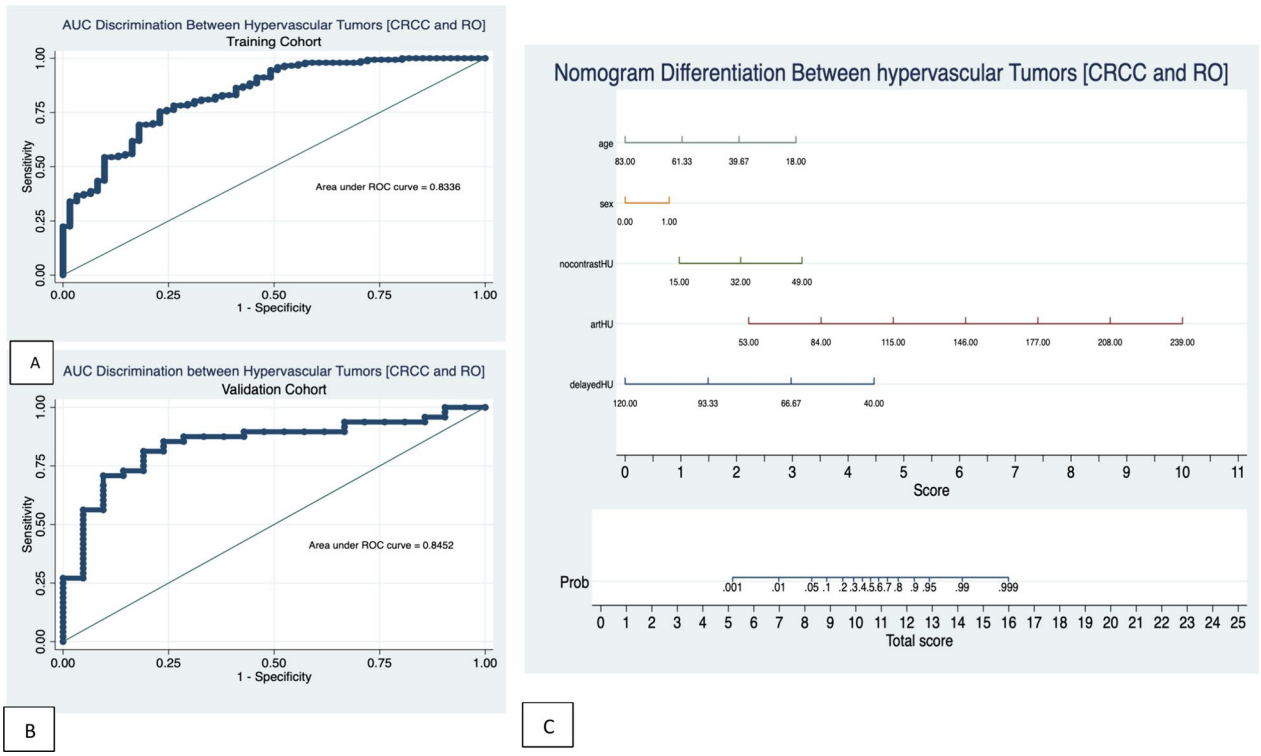

Fig. 4 A,B, and C: **A** AUC of the training cohort with accuracy = 0.83 for discrimination between hypervascular masses including CRCCC and RO. **B** AUC of the validation cohort with accuracy = 0.85 for discrimination between hypervascular masses including CRCCC and RO. **C** Nomogram using the significant predictors that can classify between two types of masses

Table 5 Significant predictors used to discriminate between hypovascular masses [ChRCC Vs. PRCC]

hypotumor	Coefficient	Std.Err	Z	P-value	[95% Conf. Interval]	
artHU	0.1729865	0.0315355	5.49	0.000	0.111178	0.2347949
delayedHU	−0.1121923	0.0314759	−3.56	0.000	−0.1738839	−0.0505007
Size	0.2166496	0.0938781	2.31	0.021	0.0326519	0.4006472
_cons	−5.170288	1.680627	−3.08	0.002	−8.464256	−1.876321

phase and the best classifiers used for tumor discrimination Fig. 6.

Discussion

Both radiologists and clinicians struggle with the diagnosis of solid benign kidney tumors without fat content. As a result, many surgeries are unnecessary [22]. Making the diagnosis and characterization of such masses is a difficult day-to-day task in clinical practice, especially given the increased incidence of discovering such masses presumably related to the growth in the use of cross-sectional imaging, especially CT.

Our study demonstrated a significant difference in tumor vascularity between the investigated renal masses. Longitudinal analysis showed that CRCC had the strongest enhancement and rapid washout, followed by RO, and both were significantly higher in vascularity than ChRCC and PRCC in all phases of the study (p value = 0.01). Multivariable analysis showed the best predictors were arterial and venous attenuations, which were positively associated with CRCC and RO, while non-contrast and delayed attenuations were negatively associated with them. The most significant clinical predictor for such discrimination was the age p value [0.009]. The mean age value was higher in CRCC and RO when compared with ChRCC and PRCC.

Based on these findings, we created our first model, which produced high accuracy with AUC values of 0.95 and 0.98 in the training and validation cohorts,

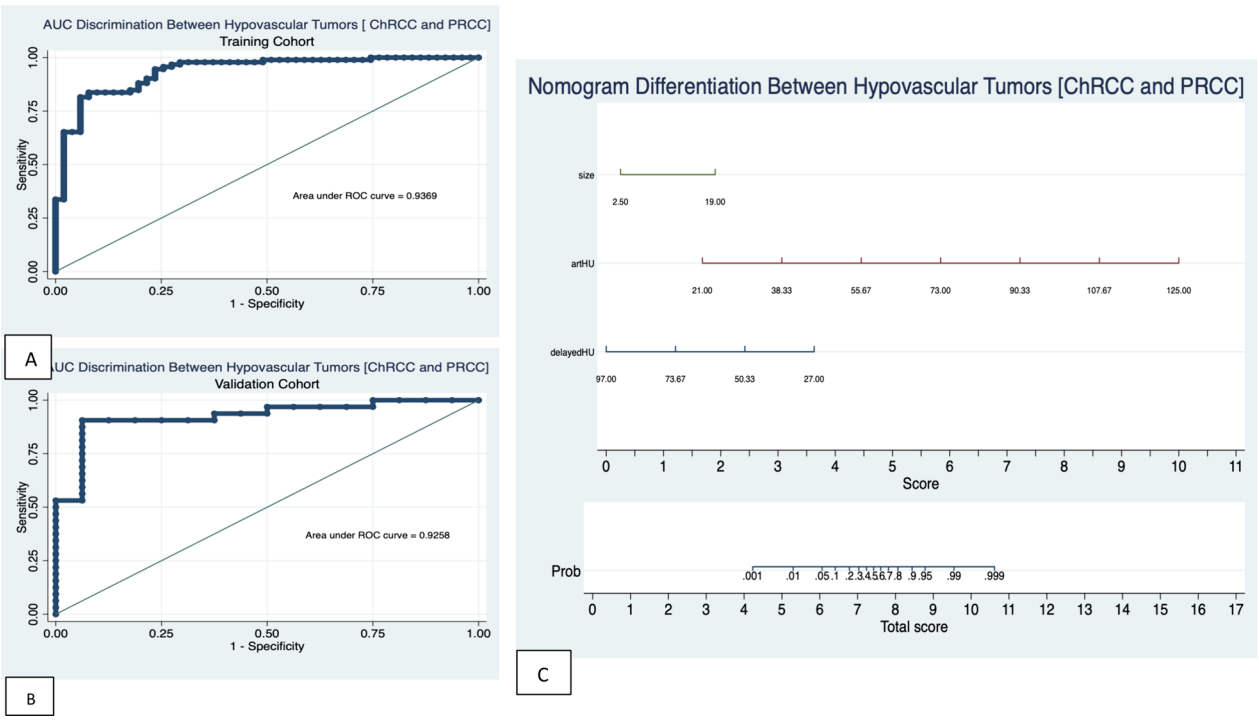

Fig. 5 A, B: **A** AUC of the training cohort with accuracy = 0.94 for discrimination between hypovascular masses including ChRCC and PRCC. **B** AUC of the validation cohort with accuracy = 0.93 for discrimination between hypovascular masses including ChRCC and PRCC. **C** Nomogram using the significant predictors that can classify between two types of masses

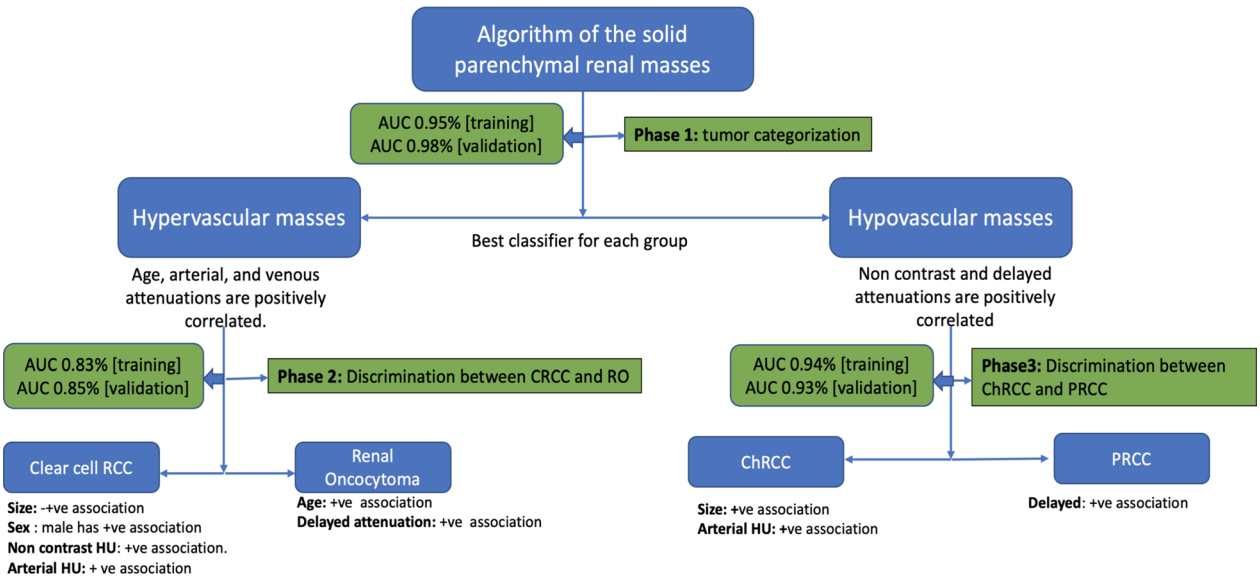

Diagram describes the best predictors and classifiers for each phase of the tumor discrimination

Fig. 6 Diagram describes the best predictors and classifiers for each phase of tumor discrimination

respectively. As a result, we begin the first step of our strategy by classifying our sample into two groups: hypovascular masses, which include ChRCC and PRCC, and hypervascular masses, that include CRCC and RO. As a result, we created our first nomogram for this type of discriminating using the aforementioned predictors.

Different researchers in the literature agreed with our findings and confirmed the pattern of substantial enhancement linked to CRCC and RO, whereas PRCC has the weakest enhancement and ChRCC has an intermediate pattern [12, 23–25]. As a result, our classification of these tumors, which includes RO, is a trustworthy method.

The second step of our approach is to discriminate between CRCC and RO. Many CT features other than enhancement have been suggested to be related to RO, such as the central stellate scar, and segmental enhancement inversion [SEI] [26–29]. However, both features are not diagnostic for RO or distinguishable from other subtypes of RCC [30–35]. For these reasons, we rely on the degree of enhancement and the significant clinical predictors to build our second model.

Our results demonstrated the size, and venous attenuation showed no significant association for such discrimination. Older age is associated with renal oncocytoma compared with CRCC, while sex, non-contrast, and arterial HU were positively associated with CRCC. The male gender had twice the odds of being associated with CRCCC compared with the RO. Combining age and sex with CT attenuation other than venous phase produced the best model. AUC values of [0.83] in the training set and [0.85] in the validation cohort represent the total accuracy of this model at this stage. Therefore, we developed the second Nomogram for this phase using the above significant predictors.

Our analysis is in good agreement with the literature in many points, seventh decade is a peak incidence period associated with RO compared with other types of RCC [25]. Although the reported variable degree of enhancement of RO is based on many studies, RO seems to show a strong enhancement like CRCC, with less washout when compared with CRCC [20, 25–27]. However, the current results are not in complete agreement with Pano et al. [36], who examined a small sample size of RO, just 13 cases against 84 cases of different types of RCC, of which 52 were clear cell and 25 were low-grade, including papillary and chromophobe RCCs. They reported that there is no significant difference between the mean enhancement of all types of RCC and RO in the corticomedullary phase. Additionally, RO showed higher enhancement in the nephrographic and excretory phases than RCC, including CRCC. These discrepancies are likely due to the small sample size used for RO and other subtypes of RCC, making the statistical significance assessment not appropriate or reliable. Additionally, they considered PRCC and ChRCC as one low-grading group, which is not reliable due to the significant enhancement difference between PRCC and ChRCC. Furthermore, they did not indicate how many cases for each subtype they had.

On the other hand, Pierorazio et al. [37] with similar sample size to Pano et al. agreed with our results as reported CRCC and RO had the higher peaks of enhancement especially in the corticomedullary and nephrographic phases, respectively, compared with PRCC and ChRCC. Moreover, other studies are supporting our results and concluded that CRCC and RO had the highest enhancement changes compared with ChRCC and PRCC and the last has the least degree of enhancement [11, 38].

Separating ChRCC and PRCC is the third phase in our methodology. During this phase, only size, arterial, and delayed attenuations represent the best classifier, with AUC values of 0.94 and 0.93 in the validation and training cohorts, respectively. Size and vascular attenuations had a favorable correlation with ChRCC. On the other hand, delayed attenuations demonstrated a favorable correlation with PRCC. These patterns of enhancement suggest that PRCC has almost progressive enhancement, particularly when contrasted to ChRCC in the delayed phase. Widespread agreement on this pattern of PRCC enhancement has been found in the literature [11, 25, 38–41], confirming our findings and giving a clear explanation for the high AUC [94%].

The present study has some limitations. First, due to its retrospective nature, it could have a selection bias; however, this study design provided us with this large number in each category. Secondly, being a single-center study, this necessitates being implemented for validation with a multicenter project, preferably a prospective study design. Third, this study does not include low fat angiomyolipoma which has a low incidence in our target sample make it unsuitable for statistical analysis which favors multicenter study.

Conclusion

In conclusion, this study presents a new and simple analytical approach using a large sample size of RCC subtypes and RO based on MDCT findings and clinical parameters and indicates that the provided models can differentiate between RCC and RO with multiphase analysis with high accuracy. Furthermore, the radiologists can simply apply the provided algorithm Fig. 6 during the daily practice to enhance the interpretation accuracy regarding the subtype discrimination. Additionally, these results can present additional insights and future

recommendations for research work, taking into consideration the current apply of radiomics features and machine learning models [42–44].

Abbreviations

CRCC	Clear cell renal cell carcinoma
Ro	Renal oncocytoma
ChRCC	Chromophobe renal cell carcinoma
PRCC	Papillary renal cell carcinoma
CT	Computed tomography
RCC	Renal cell carcinoma

Acknowledgements
Not applicable.

Author contributions
HS was responsible for the idea, planning for study design and performed the statistical analysis with substantial involvement in the writing and reviewing the whole manuscript. DE was responsible for collection of the data and interpreting CT Images, in addition to writing the manuscript. HA was responsible for organizing the data and sharing in analysis as well as writing the manuscript. TE shared in image interpretation, wrote and reviewed the manuscript.

Funding
Nothing to be disclose.

Availability of data and materials
The datasets used and/or analyzed during the current study are available from the corresponding author on reasonable request.

Declarations

Ethics approval and consent to participate
This retrospective cohort study was approved by Institutional consent from the board of Faculty of Medicine Mansoura University, Egypt. IRB number is R.22.02.1629

Consent for publication
Informed consent was waived.

Competing interests
The authors declare that they have no competing interests.

Author details
[1]Radiology Department, Urology and Nephrology Center, Mansoura University, EL Gomhorea Street, Mansoura, Egypt. [2]Radiology Department, Student Hospital, Mansoura University, Mansoura, Egypt.

Received: 30 November 2023 Accepted: 26 June 2024
Published online: 11 July 2024

References

1. Siegel RL, Miller KD, Jemal A (2018) Cancer statistics (2018). CA Cancer J Clin 68:7–30
2. Society AC (2018) Cancer facts & figures (2018). Cancer Facts Fig
3. Kovacs G, Akhtar M, Beckwith BJ et al (1997) The Heidelberg classification of renal cell tumours. J Pathol 183:131–133
4. Ishigami K, Jones AR, Dahmoush L, Leite LV, Pakalniskis MG, Barloon TJ (2015) Imaging spectrum of renal oncocytomas: a pictorial review with pathologic correlation. Insights Into Imaging 6(1):53–64
5. Pedrosa I, Sun MR, Spencer M et al (2008) MR imaging of renal masses: correlation with findings at surgery and pathologic analysis. Radiographics 28:985–1003
6. Davidson AJ, Hayes WS, Hartman DS, McCarthy WF, Davis CJ (1993) Renal oncocytoma and carcinoma: failure of differentiation with CT. Radiology 186:693–696
7. Choudhary S, Rajesh A, Mayer NJ, Mulcahy KA, Haroon A (2009) Renal oncocytoma: CT features cannot reliably distinguish oncocytoma from other renal neoplasms. Clin Radiol 64:517–522
8. Silverman SG, Israel GM, Trinh QD (2015) Incompletely characterized incidental renal masses: emerging data support conservative management. Radiology 275(1):28–42
9. Rosenkrantz NE, Wehrli J, Melamed SS, Taneja MBS (2014) Renal masses measuring under 2 cm: pathologic outcomes and associations with MRI features. Eur J Radiol 83(8):1311–1316
10. Escudier B, Porta C, Schmidinger M et al (2016) Renal cell carcinoma: ESMO clinical practice guidelines for diagnosis, treatment and follow-up. Ann Oncol 27(Suppl. 5):v58–v68
11. Bird VG, Kanagarajah P, Morillo G et al (2011) Differentiation of oncocytoma and renal cell carcinoma in small renal masses (< 4 cm): the role of 4-phase computerized tomography. World J Urol 29:787–792
12. Lee-Felker SA, Felker ER, Tan N et al (2014) Qualitative and quantitative MDCT features for differentiating clear cell renal cell carcinoma from other solid renal cortical masses. Am J Roentgenol 203:W516–W524
13. Elsayed Sharaf D, Shebel H, El-Diasty T et al (2022) Nomogram predictive model for differentiation between renal oncocytoma and chromophobe renal cell carcinoma at multi-phasic CT: a retrospective study. Clin Radiol 77(10):767–775
14. Kocak B, Yardimci AH, Bektas CT et al (2018) Textural differences between renal cell carcinoma subtypes: machine learning-based quantitative computed tomography texture analysis with independent external validation. Eur J Radiol 107:149–157
15. Bektas CT, Kocak B, Yardimci AH, Turkcanoglu MH, Yucetas U, Koca SB, Erdim C, Kilickesmez O (2019) Clear cell renal cell carcinoma: machine learning-based quantitative computed tomography texture analysis for prediction of Fuhrman nuclear grade. Eur Radiol 29(3):1153–1163. https://doi.org/10.1007/s00330-018-5698-2
16. Kocak B, Ates E, Durmaz ES, Ulusan MB, Kilickesmez O (2019) Influence of segmentation margin on machine learning-based high-dimensional quantitative CT texture analysis: a reproducibility study on renal clear cell carcinomas. Eur Radiol 29(9):4765–4775
17. Bhandari A, Ibrahim M, Sharma C, Liong R, Gustafson S, Prior M (2020) CT-based radiomics for differentiating renal tumours: a systematic review. Abdom Radiol 46(5):2052–2063
18. Larue RT, Defraene G, De Ruysscher D, Lambin P, van Elmpt W (2017) Quantitative radiomics studies for tissue characterization: a review of technology and methodological procedures. Br J Radiol 90(1070):20160665
19. Zwanenburg A, Vallières M, Abdalah MA et al (2020) The image biomarker standardization initiative: standardized quantitative radiomics for high-throughput image-based phenotyping. Radiology 295(2):328–338
20. Paño B, Soler A, Goldman DA et al (2020) Usefulness of multidetector computed tomography to differentiate between renal cell carcinoma and oncocytoma. A model validation. Br J Radiol. 93(1115):20200064
21. Paño B, Macías N, Salvador R et al (2016) Usefulness of MDCT to differentiate between renal cell carcinoma and oncocytoma: development of a predictive model. AJR Am J Roentgenol 206(4):764–74
22. Shebel HM, Al-Natour MS, Elsamaloty H (2015) Cross-sectional imaging of the kidney. In: Elsayes KM (ed) Cross-sectional imaging of the abdomen and pelvis. Springer, New York
23. Young H, Coy HJK et al (2017) Performance of relative enhancement on multiphasic MRI for the differentiation of clear cell renal cell carcinoma (RCC) from papillary and chromophobe RCC subtypes and oncocytoma. AJR Am J Roentgenol 208(4):812–819
24. Kim MH, Lee J, Cho G, Cho KS, Kim J, Kim JK (2013) MDCT-based scoring system for differentiating angiomyolipoma with minimal fat from renal cell carcinoma. Acta Radiol 54(10):1201–1209
25. Sasaguri K, Takahashi N (2018) CT and MR imaging for solid renal mass characterization. Eur J Radiol 99:40–54. https://doi.org/10.1016/j.ejrad.2017.12.008
26. Quinn MJ, Hartman DS, Friedman AC et al (1984) Renal oncocytoma: new observations. Radiology 153:49–53
27. Jasinski RW, Amendola MA, Glazer GM, Bree RL, Gikas PW (1985) Computed tomography of renal oncocytomas. Comput Radiol 9:307–314
28. Kim JI, Cho JY, Moon KC, Lee HJ, Kim SH (2009) Segmental enhancement inversion at biphasic multidetector CT: characteristic finding of small renal oncocytoma. Radiology 252:441–448

29. Woo S, Cho JY, Kim SH, Kim SY (2013) Comparison of segmental enhancement inversion on biphasic MDCT between small renal oncocytomas and chromophobe renal cell carcinomas. AJR Am J Roentgenol 201:598–604
30. Schieda N, McInnes MD, Cao L (2014) Diagnostic accuracy of segmental enhancement inversion for diagnosis of renal oncocytoma at biphasic contrast enhanced CT: systematic review. Eur Radiol 24(6):1421–1429
31. Millet I, Doyon FC, Hoa D et al (2011) Characterization of small solid renal lesions: can benign and malignant tumors be differentiated with CT? AJR Am J Roentgenol 197(4):887–896
32. O'Malley ME, Tran P, Hanbidge A, Rogalla P (2010) Small renal oncocytomas: is segmental enhancement inversion a characteristic finding at biphasic MDCT? AJR Am J Roentgenol 199(6):1312–1315
33. McGahan JP, Lamba R, Fisher J et al (2011) Is segmental enhancement inversion on enhanced biphasic MDCT a reliable sign for the noninvasive diagnosis of renal oncocytomas? AJR Am J Roentgenol 197(4):W674–W679
34. Cornelis F, Tricaud E, Lasserre AS et al (2014) Routinely performed multiparametric magnetic resonance imaging helps to differentiate common subtypes of renal tumors. Eur Radiol 24(5):1068–1080
35. Dhyani M, Grajo JR, Rodriguez D et al (2017) Aorta-Lesion-Attenuation-Difference (ALAD) on contrast-enhanced CT: a potential imaging biomarker for differentiating malignant from benign oncocytic neoplasms. Abdom Radiol 42(6):1734–1743
36. Paño B, Macías N, Salvador R et al (2016) Usefulness of MDCT to differentiate between renal cell carcinoma and oncocytoma: development of a predictive model. AJR Am J Roentgenol 206(4):764–74
37. Pierorazio PM, Hyams ES, Tsai S et al (2013) Multiphasic enhancement patterns of small renal masses (≤4 cm) on preoperative computed tomography: utility for distinguishing subtypes of renal cell carcinoma, angiomyolipoma, and oncocytoma. Urology 81(6):1265–71
38. Moldovanu CG, Petresc B, Lebovici A et al (2020) Differentiation of clear cell renal cell carcinoma from other renal cell carcinoma subtypes and benign oncocytoma using quantitative MDCT enhancement parameters. Medicina (Kaunas) 56(11):569
39. Shebel HM, Elsayes KM, Sheir KZ et al (2011) Quantitative enhancement washout analysis of solid cortical renal masses using multidetector computed tomography. J Comput Assisted Tomography 35(3):337–342. https://doi.org/10.1097/RCT.0b013e318219f92b
40. Zhang J, Lefkowitz RA, Ishill NM et al (2007) Solid renal cortical tumors: differentiation with CT. Radiology 244:494–504
41. Coy H, Young JR, Douek ML, Brown MS, Sayre J, Raman SS (2017) Quantitative computer-aided diagnostic algorithm for automated detection of peak lesion attenuation in differentiating clear cell from papillary and chromophobe renal cell carcinoma, oncocytoma, and fat-poor angiomyolipoma on multiphasic multidetectorcomputed tomography. Abdom Radiol 42:1919–1928
42. Rundo L, Beer L, Ursprung S et al (2020) Tissue-specific and interpretable sub-segmentation of whole tumour burden on CT images by unsupervised fuzzy clustering. Comput Biol Med 120:103751
43. Mottola M, Ursprung S, Rundo L et al (2021) A Reproducibility of CT-based radiomic features against image resampling and perturbations for tumour and healthy kidney in renal cancer patients. Sci Rep 11:11542
44. Könik A, Miskin N, Guo Y, Shinagare AB, Qin L (2021) Robustness and performance of radiomic features in diagnosing cystic renal masses. Abdom Radiol. https://doi.org/10.1007/s00261-021-03241-2

Publisher's Note